Estimation of the Quality of spot welding electrode tips in automotive industry in real time using digital image processing and image segmentation techniques

Abdulwanis Abdulhadi, Ahmed Ahtaiba
Department Electrical and electronics engineering
University of Sirte
Libya-Sirte

wanis92002@yahoo.co.uk

Abstract: **-** The image segmentation algorithm is the most challenging step and requires more computers processing power than the boundary filtering, and the Cullen et al's method, which used the Cullen et al's method to determine the electrodes tip width automatically in the automotive industry in real time. Spot welding is used extensively in the automotive industry. The quality of an individual spot weld is a major concern due to the heavy reliance on their use in the manufacture of motor vehicles. The main parameters that control the quality of a spot weld are current, voltage, welding force, welding time, and the quality of welding electrodes. The condition of the welding electrodes plays a major part in determining the quality of a spot weld. For example, excessive electrode wear can occur during the welding process and can cause weakening in the weld nuggets. As the number of welds increases, the electrode tip wears down and so the contact area between electrode tip and work piece increases. In order to determine the quality of the welding electrodes, a machine vision approach is employed, where images of the electrode tips in real time are captured and are processed using various image-processing algorithms. These algorithms can be used to automatically measure the electrode tip width and hence assess the quality of the electrodes tip in real time. The quality of spot welding electrode tips, namely flat-shaped, is assessed here using image processing techniques. For the tip type, a database of 250 images is used to test the performance of the tested algorithms. Also the tip width in these 250 images is determined manually by counting the number of pixels using an image editor such as Microsoft Paint. An excellent agreement is found between these manual and automatic methods. The tip width for an electrode is measured by first grabbing an image showing the electrode. The electrode in the image is then extracted using an image segmentation algorithm. Then the boundary of the electrode is determined and filtered. The Cullen et al's method is subsequently applied, which uses the filtered boundary to determine the tip width. A number of image segmentation and boundary filtering algorithms have been used to determine the tip width automatically. For flat tip electrode, the combination of the region growing image segmentation, Minimum Perimeter Polygon, and Cullen et al's techniques was capable of automatically determining the tip width for 250 images with a root mean square error 7.5 % of the tip width. For dome tip electrode, the combination of Snake active contours method image segmentation, Fourier transform boundary descriptor and Cullen et al's method techniques was capable of automatically determining the tip width for 250 images with a root square error 2.9% of the tip width.

Key-Words: **-** *Spot welding, Image segmentation algorithms and representation*

I. INTRODUCTION

Resistance spot welding (sometimes referred to as "resistance welding") is a quick and easy way of joining two materials [1, 2]. The most common application of resistance spot welding is in the automotive industry as it lends itself to rapid, high-volume welding applications, of which this is a prime example. It can be used to join together two or more metallic worksheets. This is achieved by means of the welding. electrodes, which are placed into forcible contact on either side of the work pieces that are to be joined, and then by passing electrical current through the electrodes, typically the sheets are in the 0.5 to 3 mm (0.020 to 0.12 in) thickness range and sheets in order to generate heat and cause fusion at the faying interface of the worksheets. This is achieved by means of the welding electrodes, which are placed into forcible contact on either side of the work pieces that are to be joined, and then by passing electrical current through the electrodes and sheets in order to generate heat and cause fusion at the faying interface of the worksheets. Each weld sequence consists of four main stages: 1) clamping of the work; 2) applying the weld force required for welding [3, 4]; 3) applying the weld current necessary for fusion of the work pieces [5,6]; 4) a final retraction of the electrodes after the molten nugget has solidified. This process is illustrated in Fig1

When melting has occurred, the current is removed and the original pressure is held for a short period of time thereby allowing the metals to solidify. At this point the weld ''nugget'' is formed. This nugget is the point at which the two metals are joined together and the volume of this joint is of paramount importance to the final strength of the weld. If this nugget is too small then the weld is likely to be weak and the risk of the two metals separating during use is significantly increased. An important factor in determining the size of the weld nugget is the surface area of the electrodes at the point of contact.

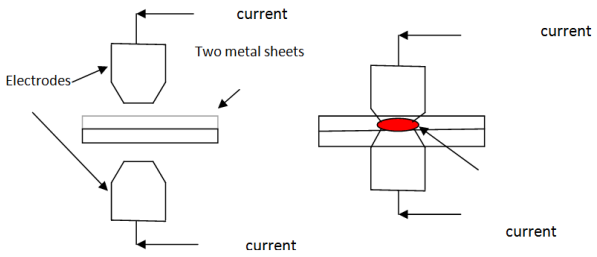

Fig.1. How weld nuggets are formed.

Degradation of the electrode tips results in a loss of their ability to perform their functions. The three functions of a resistance welding electrode are to provide the necessary weld force, weld current density, and cooling. Typical electrode degradation occurs when the tip diameter of the electrode grows too large to convey adequate current density to the work piece. This process is illustrated in Fig 3. As the diameter of the tip (tip width T_p) increases, so does the surface area of the tip. This results in a reduced current density and means that the heat generated during the welding process is insufficient, hence resulting in a smaller weld nugget [7, 8].

In this paper, we propose using image processing algorithms to determine the tip width automatically. Firstly, we capture an image for the electrode. Then we use an image segmentation algorithms are canny algorithm, region grown algorithm and graph theory algorithm to extract the electrode from the image [9, 10]. The boundary of the electrode object in the segmented image is then determined. This boundary is filtered using for example, Fourier transform boundary descriptor algorithm or minimum perimeter polygon methods [10]. Finally, the Cullen et al's method to determine the electrodes tips width automatically from the filtered boundary.

II. FIND TIP WIDTH

Firstly, we introduce Cullen et al's method to determine the tip width automatically [8]. Fig.2 shows an image that contains a flat tip and indicates its parameters such as the tip width T_p and the electrode width C_p.

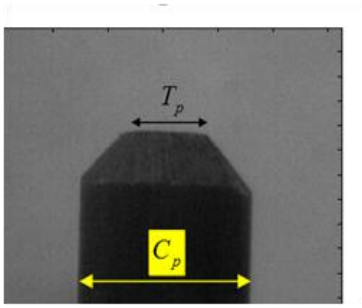

Fig.2 An image shows a flat real tip.

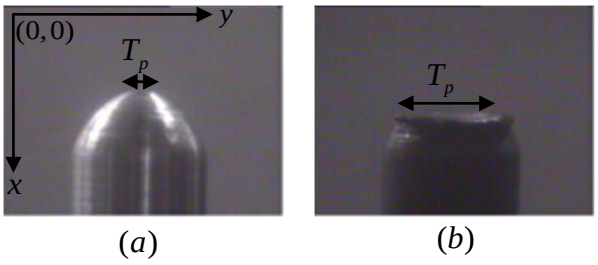

Fig. 3. (a) new electrode dome tip, (b) weared electrode tip.

Fig.4 shows an image that contains the boundary of the ideal flat tip.

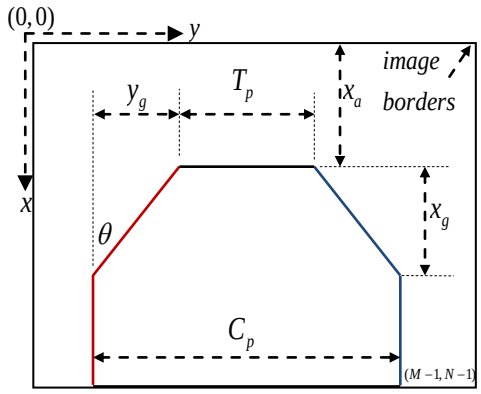

Fig. 4 An image shows the boundary of the tip and tip's parameters

Suppose that the size of both the tip image and the boundary image are M × N pixels. Let us process the boundary image row by row. For each row, we subtract the x coordinates of the left boundary points (shown in red colour) from the x coordinates of the right boundary points (shown in blue colour). The first x_a rows do not contain the tip boundary. The subtraction operation produces zeros as shown in Fig. 4. For the row x_a +1, the subtraction operation produces the tip width T_p. For the rows from x_a + 1 until x_a + x_g, the subtraction operation produces a line with the slope of

$$g = 2\tan\theta = \frac{C_p - T_p}{x_g} = \frac{2y_g}{x_g} \qquad (1)$$

The value of θ can be determined by measuring the gradient angle of the tip under inspection or extracted this value from the manufacturer datasheet. Similarly, the value of electrode width C_p can be measured or extracted from the manufacturer datasheet. For the tip shown in Fig. 5, the gradient angle is close to 45°. For the rows from x_a + x_g + 1 until M, the subtraction operation produces the value of C_p. The results of the subtraction operation are indicated in the 2D graph shown in Fig.5

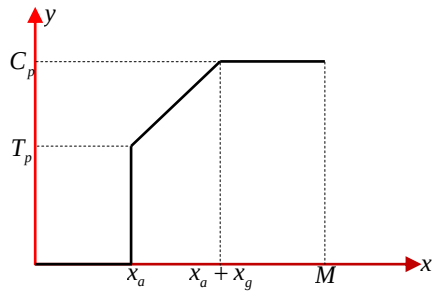

Fig.5 The profile of the tip.

The first derivative of the 2D graph in Fig.5 is calculated and is shown in Fig. 6. The first derivative of the 2D graph in Fig. 6 is calculated and is shown in Fig.6.

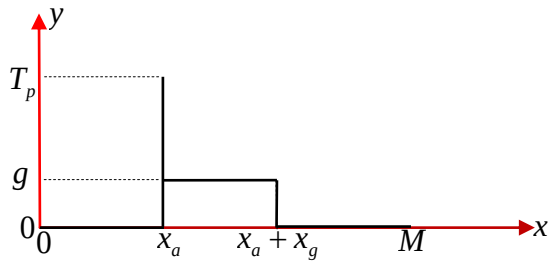

Fig.6 The first derivative of the tip profile shown in Fig.5

The width of the tip is determined as follows. The derivative of the tip profile is thresholded using the threshold g. The value of the tip gradient g is priori known. Then the numbers of points whose values are larger g than is determine and this number is assigned to x_g. The tip width is then determined using Equation (1).

III. SEGMENTATION ALGORTHM FOR AUTOMATIC DETERMINATION OF THE TIP WIDTH IMGE IN FLAT TIP

To determine the diameter and the width of the tip from the image of the tip, it is necessary to produce an outline of the tip. This task can be carried out by separating the electrode in the image from the image background and this procedure can be carried out by using image segmentation techniques. In this paper, we have used three segmentation algorithms for comparison: Canny, region growing and graph theory. Additionally, we have used three image representation algorithms: Cullen et al's method, Fourier transform and minimum perimeter polygon. The tip determination technique requires one image segmentation algorithm and at least one image representation algorithm.

There are nine different potential combinations of the image segmentation and image representation algorithms can be used. For example, region growing and minimum perimeter polygon, region growing and Fourier transform and so on. We have tested the performance of these nine combinations and we found that they work very well for the images we have as shown below in Figures 8-25.

All the algorithms work correctly on a set of two hundred and fifty images that we have. All these images have been captured with great care under laboratory conditions of different background and illumination.

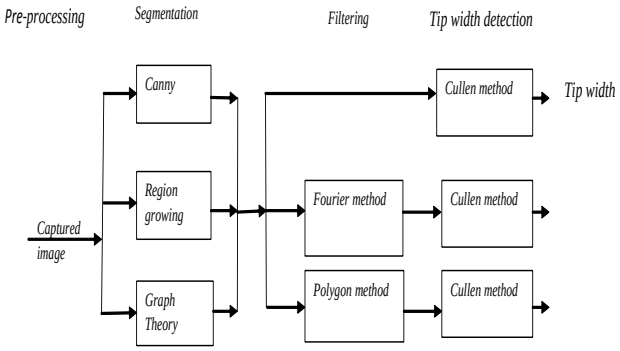

Fig.7 The various possible combinations of the algorithms that were used to automatically detect the width of a flat electrode tip.

We have tested the Canny, seeded region growing and Graph Theory algorithms using 250 images. All the three methods segment the 250 images successfully. As indicated in Fig7, there are nine combinations of the image segmentation and boundary filtering algorithms that can be used to extract the tip width. In this section, we will use these nine combinations to extract the tip width automatically for the 250 image set in the image library. Then the tip width will be extracted manually for these 250 images by pixel counting in an image editor. The threshold limit on the maximum allowed tip width as recommended by British standards in automatically industry [Prestar EN61WEERING-UK] [13, 15] is $6.5\sqrt{t}$, where t is the thickness of the welded metal in 0.8 mm. Consequently, the "usability threshold" for the tip width in pixels is approximately 105 pixels or lower. The main aim of this paper is to automatically determine if the tip width is below or above the "usability threshold", which we set here to be 105 pixels. When the tip width is above the threshold, the electrode will be considered to be "non-usable" and at this point it therefore should be replaced. We will calculate the mathematical differences between the tip widths that were found automatically using each of the possible combinations of algorithms and those that were obtained manually. The root mean square error of this mathematical difference is then calculated. We will consider the algorithm that has the smallest root mean square error as being the "best algorithm" amongst the nine combinations which are being used to automatically extract the tip width

.

A. *Canny and Cullen et al's method*

In this first combination, the canny method is used for image segmentation and the Cullen et al's method is used to automatically find the tip width in pixels for the two-hundred and fifty images in the images experiments. This is the combination that is proposed by Cullen et al's method in [8]. The automatically found tip widths are plotted in Fig 8 using red colour. Fig 8 also shows the tip width as determined manually, shown in blue colour for all of the two-hundred and fifty images. Fig.9 shows the mathematical difference between the manual and automatic determination of the tip width in pixels. There is a good agreement between the manually and the automatically obtained tip width for the first 105 images (except for a few images at the beginning). The error that occurs for these few images at the beginning is caused by the fact that the top of the tip is slightly rounded. This is shown as case "a" in Fig.9. For the images with indices between 100 and 160, the automatically estimated tip size is larger than that of the manually measured tip. This is mainly due to the presence of protrusions in the electrode tips. This is shown as case "b" in Fig .9. This large error occurs when the tip width is larger than the usability threshold. Consequently, this error does not produce any false alarms. If the protrusion has occurred when the tip width is below the usability threshold, then this algorithm may consider it to be non-usable and may in this case produce a false positive. This can degrade the reliability of the algorithm. For the images with indices larger than 161, the results for the automatically estimated tip size is close to that of the manually measured tips widths. This algorithm automatically does not produce false positive, but it produces some few false negative rate might be 5 in 100 images below usability threshold when the tip width is close to the usability threshold.

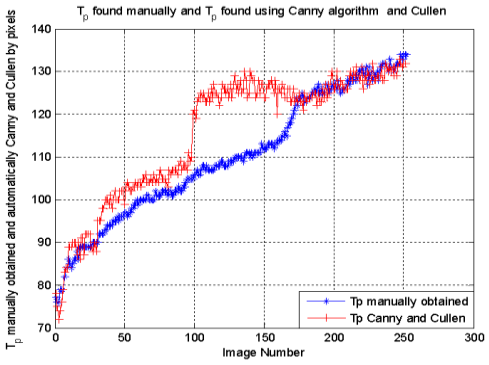

Fig.8 Determining the tip width in pixels manually (shown in blue colour) and automatically using the Canny Algorithm and Cullen method (shown in red).

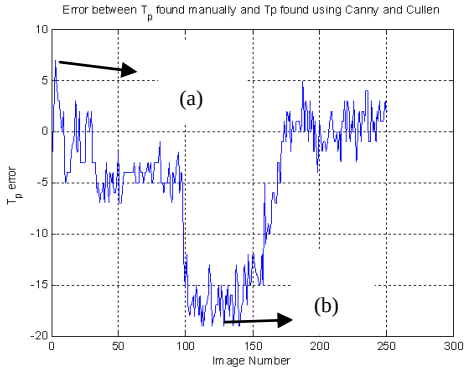

Fig.9 The difference between estimating the tip width manually and automatically using the Canny algorithm and Cullen et al. methods

B. *Canny, Fourier transform and Cullen et al's method*

In the second combination of techniques, the electrode is extracted for all images in the 250 image experiments using the Canny algorithm method, determining the boundary of the electrode. The boundary is then filtered using the Fourier transform boundary descriptor method. *P* here is set to a value of 110. The filtered boundary is then applied to the Cullen et al's method for automatically determining the tip width. The results are shown in Fig 8 indicated by the red colour trace. The tip width was also extracted manually and the results are also shown in Fig 10 indicated by the blue colour trace. The mathematical differences between the results that were produced manually and those that were produced using this automatic method are shown in Fig.11. Fig.11(a) shows an example of a large error that has occurred in automatically determining the tip width. This error has been introduced due to the presence of the noticeable protrusion in the tip and the consequent failure of the Fourier transform method in terms of reducing the error that is introduced by this protrusion. On the other hand, Fig .11(b) shows an example of a small error that was achieved using this combination to automatically determine the tip width. In this section, the use of the Fourier transform approach to filter out the boundary of the tip has decreased the reliability in determining the tip width. This can be confirmed by a comparative visual inspection of the respective error graphs that are shown for the previous combination of algorithms as given in Fig9 and the current combination of algorithms which is shown in Fig.11. In this combination, this automatically algorithm does not produce false positive, but it produces some few false negative rates might be 7 in 100 images below usability threshold when the tip width is close to the usability threshold.

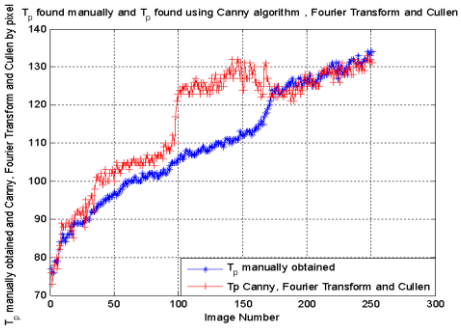

Fig.10 Determining the tip width in pixels manually (shown in blue colour) and automatically using the Canny, Fourier transform and Cullen et al.'s methods (shown in red).

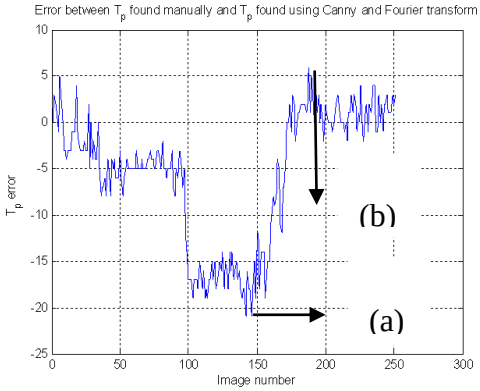

Fig.11 The difference between estimating the tip width manually and automatically using the Fourier transform and Cullen methods, (a) large error, (b) small error

C. Canny, Minimum Perimeter Polygon and Cullen et al's method

In this combination, the electrode in the 250 images is extracted using the Canny algorithm. The boundary is then filtered using the Minimum Perimeter Polygon algorithm (MPP) [1, 10]. The cell size is set here to a value of 2 and this result in a high resolution boundary with some of the noise being removed. The filtered boundary is then applied to Cullen et al.'s method to determine the tip width. The results are shown in Fig 12 using the red colour trace. The tip width is also extracted manually and the results are also shown in Fig 12 using the blue colour trace. The mathematical differences between the results that were produced manually and those that were produced automatically using this combination of algorithms are shown in Fig.13. Fig.13(b) shows a case when there is a "large" error between the manual and automatic determination of the tip width; however the automatic tip width is larger than the manually determined tip width. A case of "moderate" error in tip width determination is shown in Fig.13 case (a). A visual inspection of Figs.11 and 13 reveals that there is large error in automatically determining the tip width. The use of the Minimum Perimeter Polygon algorithm has not improved the performance of Cullen et al's method. The error exceeds 20 pixels and this is not acceptable. On the other hand, if we consider the "usability threshold" as being 105 pixels, as explained above, then this combination produces false negative rates might be 24 in 100 images below usability threshold and it does not produce false positive.

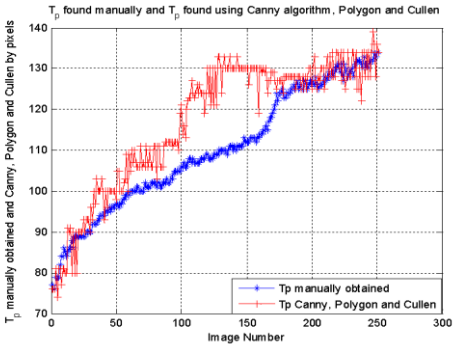

Fig.12 Determining the tip width in pixels manually (shown in blue colour) and automatically using the Canny algorithm, Minimum Perimeter Polygon and Cullen et al. methods (shown in red)

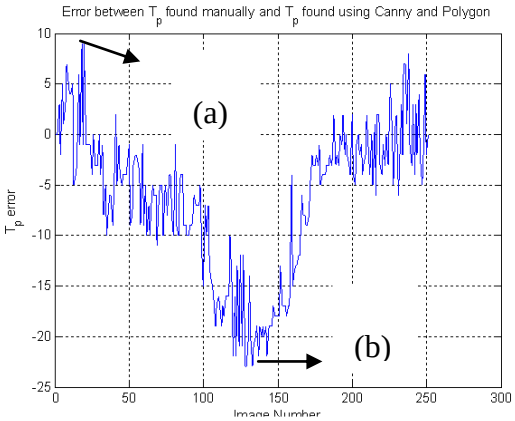

Fig.13 The differences between estimating the tip width manually and automatically using the Canny algorithm, Minimum Perimeter Polygon and Cullen et al.'s methods,

D. Region growing algorithm and Cullen et al's method

Region growing is a procedure that groups pixels, or sub-regions, into larger regions based a predefined criterion for growth [12]. The main idea is to start with a set of ''seed'' points and from these grow regions by appending to each seed those neighbouring pixels that have predefined properties similar to those of the seed. In this fourth combination, the electrode in the 250 images is extracted

using the region growing algorithm to extract the boundary of the spot welding electrode. The Cullen et al's method then uses this extracted boundary to automatically determine the tip width. The results are shown in Fig .14 using the red colour trace. The tip width is also extracted manually and the results are shown in Fig .14 using the blue colour trace. The mathematical differences between the results that were produced manually and those that were produced using this automatic method are shown in Fig.15. Fig.15 shows two cases that both exhibit large errors. Case (a) shows a large negative error, where the automatically estimated tip width is smaller than the manually measured tip width. In this case, this automatic system produces a false positive rate might be 1 in 105 images. False positive are considered to be more dangerous to system performance than a false negative, because they only cause a potential loss of an unnecessarily early tip replacement, whereas false positive imply missed faulty welds and could involve the recall of the entire output across a period of vehicle production. Fig.15 also shows another case (b), where the automatically estimated tip width is larger than the manually measured tip width. In this case, this automatic system produces a false negative rates might be 4 in 100 images below usability threshold. In this section, the use of the region growing algorithm has not improved the performance of the system as large errors are still produced.

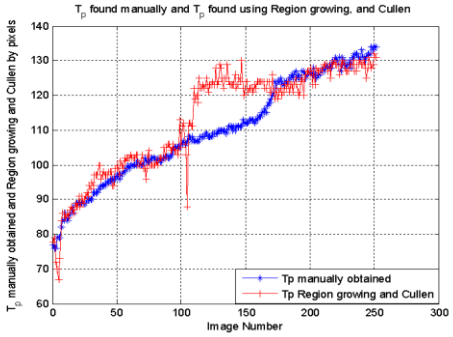

Fig..14 Determining the tip width in pixels manually (shown in blue colour) and automatically using the region growing algorithm, and Cullen et al.'s methods (shown in red).

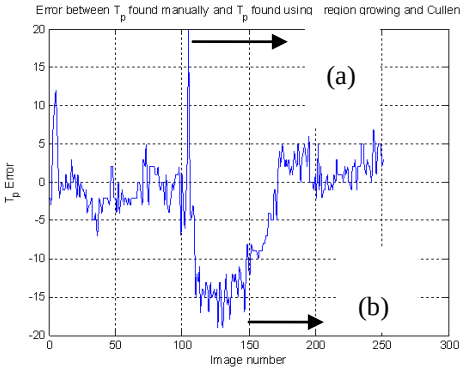

Fig.15 The difference between estimating the tip width in pixels manually and automatically using region growing algorithm and Cullen et al.'s methods,

E. Region growing, Fourier transform and Cullen et al's method

In this fifth combination, the electrode in the 250 images is extracted using the region growing algorithm in order to extract the boundary of the electrode. The boundary is then filtered using the Fourier transform boundary descriptor method. *P* is set here to a value of 110. The filtered boundary is then applied to Cullen et al.'s method for determining the tip width. The results are shown in Fig16 using the red colour trace. The tip width is also extracted manually and the results are shown in Fig16 using the blue colour trace. The mathematical differences between the results that were produced manually and those that were produced using this automatic method are shown in Fig.17. Fig.17 (a) shows a case of "medium" error between the manually and automatically determined tip width. Fig.17 (b) shows a case of "large" error between the manually and automatically determined tip width. Even though the error produced using this combination is large, it does not produce false positive. Also, this algorithm does not produce false negative for tip widths that are below the usability threshold.

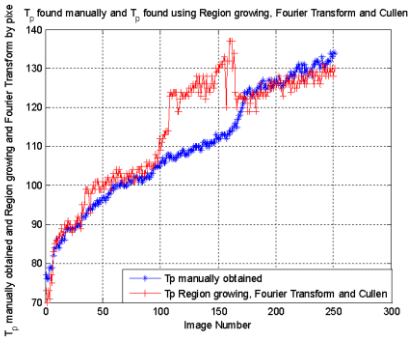

Fig.16 Determining the tip width in pixels manually (shown in blue colour) and automatically using the region growing algorithm, Fourier transform and Cullen et al.'s methods (shown in red).

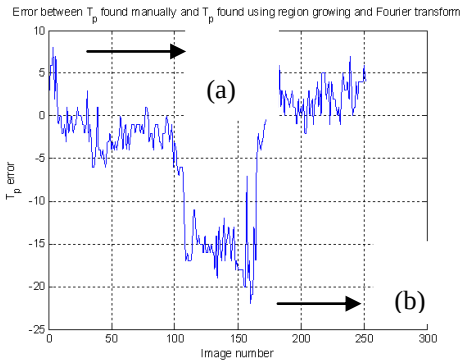

Fig.17 The difference between estimating the tip width in pixels manually and automatically using the region growing algorithm, Fourier transform and Cullen et al.'s methods,(a) medium error, (b) large error.

F. Region growing Polygon and Cullen et al's method

In this combination, the electrode in the 250 images is extracted using the region growing algorithm. The boundary is then filtered using the Minimum Perimeter Polygon algorithm [1, 10]. The cell size is set here to a value of 2. The filtered boundary is then applied to Cullen et al.'s method to automatically determine the tip width. The results are shown in Fig.18 using the red colour trace. The tip width is also extracted manually and the results are also shown using the blue colour trace in Fig.18. The mathematical differences between the results that were produced manually and those that were produced using this automatic method are shown in Fig.19. The region growing; Minimum Perimeter Polygon and Cullen case is superior because the error term for T_p is smaller than the other eight combinations. Figs.19 (a) and (b) show two cases with "medium" errors in determining the tip width. The performance of this combination is better than the other eight combinations as it produces less error. The system produces false negative rates might be 5 in 105 image within the below "usability range". Also, the Minimum Perimeter Polygon method has an excellent ability in terms of reducing the protrusion effect when measuring the tip width and root mean square error is 7.5 %. On the other hand, this algorithm shows a case of false positive and the false positive rate might be 2 in 100 images within the below usability threshold. In Fig.19 case (c) is shown false negative.

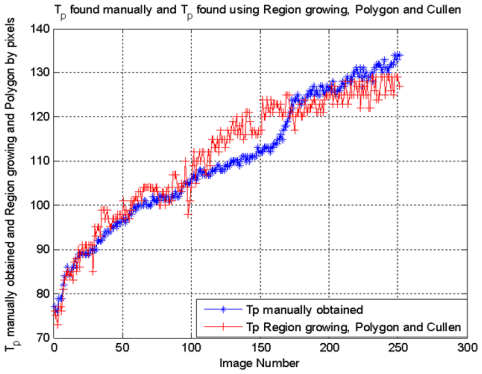

Fig.18 Determining the tip width in pixels manually (shown in blue colour) and automatically using region growing algorithm, Minimum Perimeter Polygon and Cullen et al.'s methods (shown in red).

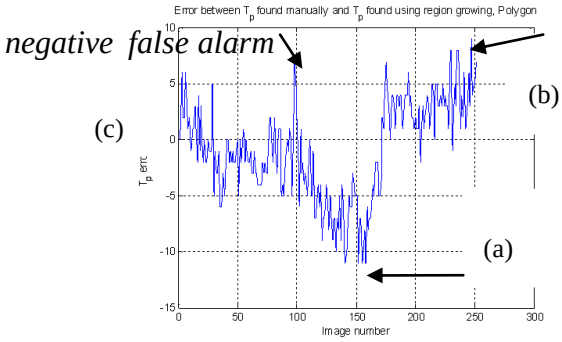

Fig.19 The error between estimating the tip width in pixels manually and automatically using the combination of Region Growing, MPP and Cullen methods; Showing three cases(a) moderate error, (b) moderate error, (c) moderate error.

G. Graph Theory algorithm and the Cullen et al's method

In this seventh combination, the electrode boundary in the 250 images is extracted using the Graph Theory segmentation algorithm [9]. The boundary is then applied to Cullen et al.'s method to automatically determine the tip width. The results are shown in Fig .20 using the red colour trace. The tip width is also extracted manually and the results are shown using the blue colour trace as shown in Fig .20. The mathematical differences between the results that were produced manually and those that were produced using this automatic method are shown in Fig.21. As shown in

Fig.21, there is large error between the manually and automatically determined tip widths. In this section, this algorithm does not produce false positive, but it produces some few false negative rate 4 in 100 images below usability threshold when the tip width is close to the usability threshold.

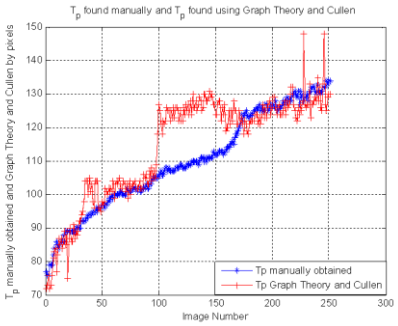

Fig.20 Determining the tip width in pixels manually Cullen et al.'s methods (shown in red).lly (shown in blue colour) and automatically using the Graph Theory algorithm an

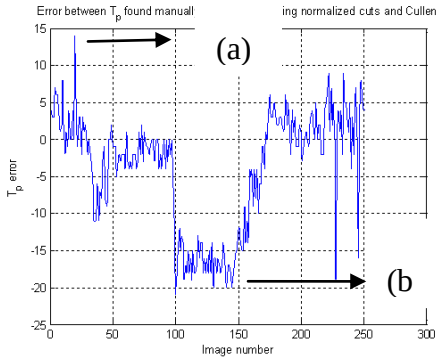

Fig.21 The error between estimating the tip width in pixels manually and automatically using the Graph Theory algorithm and Cullen et al.'s method, (a) large error, (b) large error.

H. *Graph Theory, Fourier transform and Cullen et al's method*

In this combination, the electrode boundary in the 250 images is extracted using the Graph Theory segmentation algorithm [9]. The boundary is then filtered using the Fourier transform algorithm [1, 10]. The filtered boundary is then applied to Cullen et al.'s method to automatically determine the tip width. The results are shown in Fig.22 using the red colour trace. The tip width is also extracted manually and the results are shown in Fig .20 using the blue colour trace. The mathematical differences between the results that were produced manually and those that were produced using this automatic method are shown in Fig.23. The error produced using this algorithm exceeds 60 pixels. Consequently, this combination produces the bad results out of all the combinations of algorithms that were investigated. In this section, this automatically algorithm does not produce false positive, but it produces many false negative rates might be 16 in 100 images below usability threshold when the tip width is close to the usability threshold.

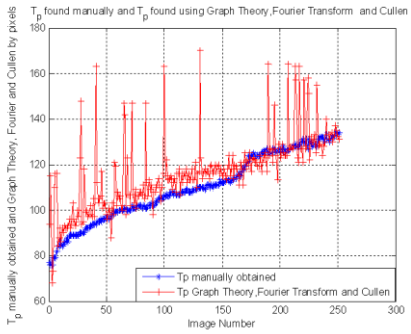

Fig.22 Determining the tip width in pixels manually (shown in blue colour) and automatically using the Graph Theory algorithm, Fourier transform and Cullen et al.'s methods (shown in red)

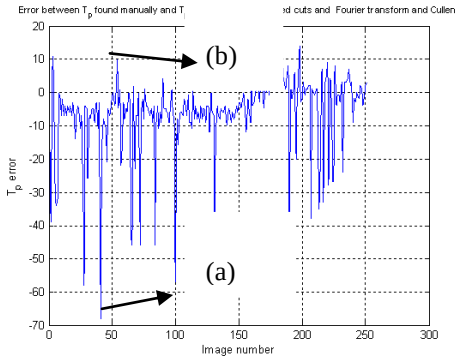

Fig.23 The error between estimating the tip width in pixels manually and automatically using the Graph Theory algorithm, Fourier transform and Cullen et al.'s methods, (a) large error, (b) large error

I. *Graph Theory, Minimum Perimeter Polygon and Cullen et al's methods*

In this last combination, the electrode boundary in the 250 images is extracted using the Graph Theory algorithm. The boundary is then filtered using the Minimum Perimeter Polygon algorithm [1, 8]. The cell size is set here to a value of 2. The filtered boundary is then applied to Cullen et al.'s method to automatically determine the tip width. The results are shown in Fig 24 using the red colour trace. The tip width is also extracted manually and the results are shown in Fig

24 using the blue colour trace. The mathematical differences between the results that were produced manually and those that were produced using this automatic method are shown in Fig 25. As shown in this figure, there is large error between the manually and automatically determined tip widths. The errors produced by this combination are large and exceed 60 pixels in magnitude. Consequently, this combination produces the second high results of false positive rate out of all the nine different combinations of algorithms that were tested. In this section, this automatically algorithm produce does not false positive below usability, but it produces many false negative rates might be 8 in 100 images below usability threshold when the tip width is close to the usability threshold.

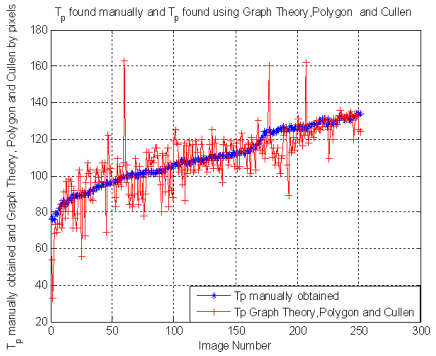

Fig 24: Determining the tip width in pixels manually (shown in blue colour) and automatically using the Graph Theory algorithm, Minimum Perimeter Polygon approach and Cullen et al.'s methods (shown in red).

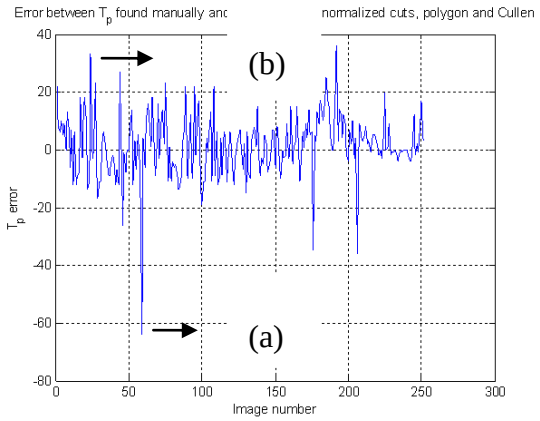

Fig 25 The error between estimating the tip width in pixels manually and automatically using the Graph Theory algorithm, Minimum Perimeter Polygon approach and Cullen et al.'s methods, (a) large error, (b) large error

IV. SEGMENTATION ALGORTHM FOR AUTOMATIC DETERMINATION 0F THE TIP WIDTH IMAGE IN DOME TIP

To determine the tip width from the tip's image, it is necessary to produce an outline of the tip. This task can be carried out by separating the electrode in the image from the image background and this procedure can be carried out by using image segmentation techniques. This can be a difficult task to do as there is noise, other objects in the image, non-uniform background illumination, shinning parts in the electrode. We carried out an exhaustive research to find an algorithm to extract the electrode in image shown in Figure 3(a) successfully [9]. Many image segmentation algorithms failed, but we found that the snake active contours algorithm can fulfil the segmentation task. We have tested the snake algorithm using 250 images and it segments them all successfully [12].

As explained above, the first derivative of the tip profile is noisy. To reduce the noise effect, the tip profile should be filtered before applying the derivative operation. We have used here two methods to filter the tip profile: Fourier transform and the minimum perimeter polygon. As indicated in Figure 26, there are three combinations of the image segmentation and image representation algorithms can be used to extract the tip width. The first combination is snake active contours and Cullen et al. method. The second combination is snake active contours, Fourier transform and Cullen et al. method. The third combination is snake active contours, minimum perimeter polygon and Cullen et al. method.

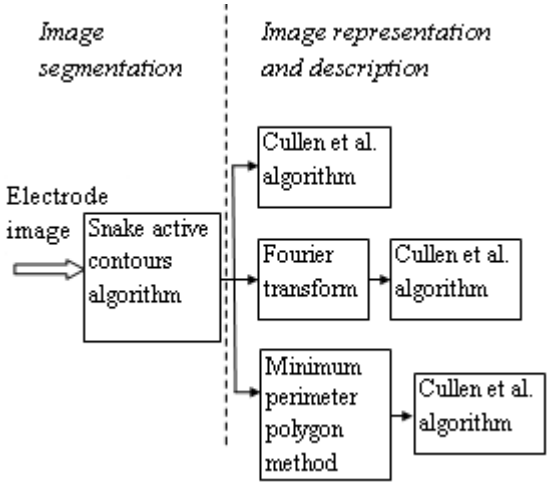

Fig.26 The various possible combinations of the algorithms that were used to automatically detect the width of a dome electrode tip.

A. *Snakes active contour and Cullen methods*

The snakes are curves defined within image domain that can move under the influence of internal forces coming from within the curve itself and external forces computed from the image data. The internal and external forces define the snakes and will conform to an object boundary or other desired features within an image. The snakes are widely used in many applications, including edge detection [21], shape modelling [22],[23], segmentation [24],[25], and motion tracking[26],[27]. In this paper, we use the parametric active contours within an image domain and allow them to move toward desired features, usually edges.

There are two key difficulties with parametric active contour algorithms. First, the initial contour must, in general, be close to the true boundary or else it will likely converge to the wrong result. The second problem is that active contours have difficulties progressing into boundary concavities [26],[27].

A traditional snake is a curve $x(s)=[x(s),y(s)], s\in[0,1]$, that moves through the spatial domain of an image to minimize the energy functional

$$E=\int_0^1 \frac{1}{2}\left[\alpha\left|x'(s)\right|^2+\beta\left|x''(s)\right|^2\right]+E_{ext}(x(s))ds \qquad (2)$$

Where α and β are weighting parameters that control the snakes tension and rigidity, respectively, and x'(x) and x''(s) denote the first and second derivatives of $x(s)$ with respect to *s*. The external energy function E_{ext} is derived from the image so that it takes on its smaller values at the features of interest, such as boundaries.

We have used the snake active contour method to segment 250 images and to determine the boundary of the electrode in these images. The segmented images are then applied to Cullen et al. method to estimate the tip width. The results are shown in Figure 27 using the red colour.In order to assess the performance of the above algorithm, we have measured the tip width for the 250 images manually and the results are shown in Figure 28 using the blue colour.

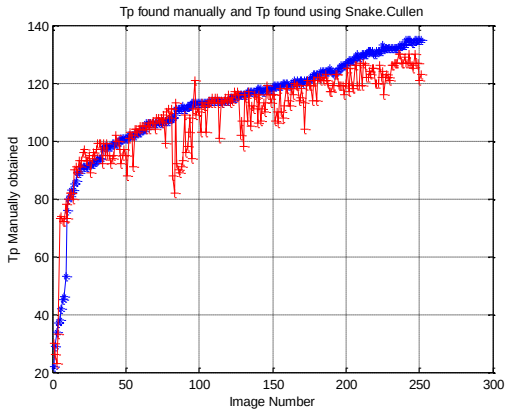

Fig. 27 Determining the tip width manually (shown in blue colour) and automatically using snake active contour and Cullen et al. methods (shown in red).

.

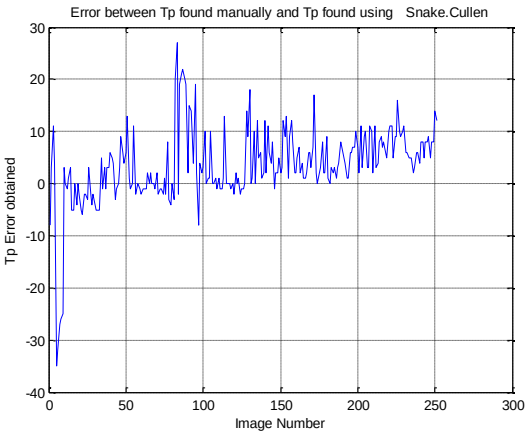

Fig.28. The error between estimating the tip width manually and automatically using snake active contours and Cullen et al. methods.

B. *Snakes active contour, Fourier transform boundary descriptor and Cullen methods*

The boundary can be filtered using Fourier transform boundary descriptor method as explained here. The *K*-point digital boundary in the *xy* plane. Starting at an arbitrary point (x_o, y_o), coordinate pairs (x_o, y_o), (x_1, y_1), (x_2, y_2),..., (x_{K-1}, y_{K-1}) are encountered in traversing the boundary in counter clockwise direction. These coordinates can be expressed in the form $x(k) = x_k$ and $y(k) = y_k$. With this notation, the boundary itself can be represented as the sequence of coordinates $s(k) = [x(k), y(k)]$, for $k = 0, 1, 2, K-1$. Moreover, each coordinate pair can be treated as a complex number as $s(k) = x(k)+ iy(k)$. That is *x* axis is treated as the real axis, and the *y* axis as the imaginary axis of a sequence of complex numbers. The discrete Fourier transform of $s(k)$ is

$$a(u)=\sum_{k=0}^{K-1} s(k)e^{-j2\pi uk/K} \qquad (3)$$

For $u = 0, 1, 2, K-1$. The complex coefficients $a(u)$ are called the Fourier descriptors of the boundary. The inverse Fourier transform of these coefficients restores $s(k)$. That is,

$$s(k)=\frac{1}{k}\sum_{u=0}^{K-1} a(u)e^{j2\pi uk/K} \qquad (4)$$

For $u = 0, 1, 2, K-1$. Suppose, however, that instead of all the Fourier coefficients, only the first *P* coefficients are used. This is equivalent to setting $a(u) = 0$ for $u > P-1$. Then we get an approximation for the boundary. The low frequency components account for the global shape of the boundary; whereas the high frequency components account for the fine details shape in the boundary.

As explained before, in the second combination the electrode in the 250 images is extracted using the snake active contour method. Also, this method determines the boundary of the electrode. The boundary is then filtered using Fourier transform boundary descriptor method. *P* is set here to 110. The filtered boundary is then applied to

Cullen et al. method to determine the tip width. The results are shown in Figure 29 using the red colour. The tip width is extracted manually and the results are shown using the blue colour. The mathematical differences between the results produced manually and using this automatic method results is shown in Figure 30.

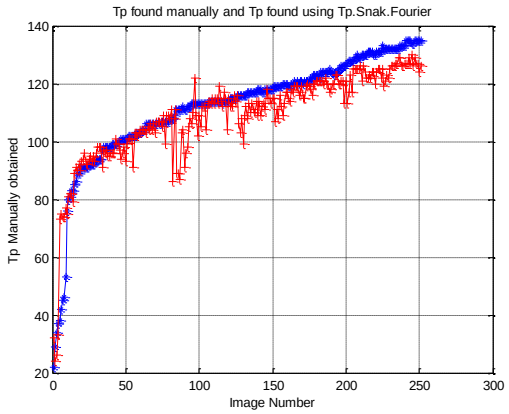

Fig. 29. Determining the tip width manually (shown in blue colour) and automatically using snake active contour, Fourier transform boundary descriptor and Cullen et al. methods (shown in red).

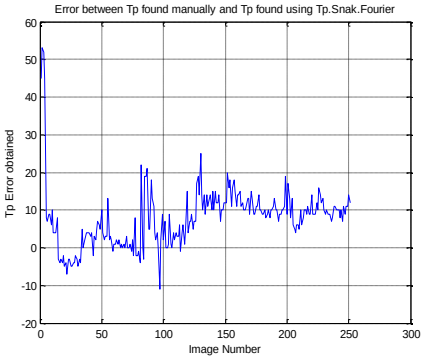

Fig.30. The error between estimating the tip width manually and automatically using snake active contours, Fourier transform boundary descriptor and Cullen et al. methods.

C. Snakes active contour , minimum perimeter polygon and Cullen methods

The boundary can be approximated can be approximated with arbitrary accuracy by a polygon. For a closed boundary, the approximation becomes exact when the number of vertices of the polygon is equal to the number of points in the boundary, and each vertex coincides with a point on the boundary. The details and the noise in the boundary can be reduced by decreasing the number of vertices.

As explained before, in the third combination the electrode in the 250 images is extracted using the snake active contour method. The boundary is then filtered using the minimum perimeter polygon [9]. The cell size is set to 2 and this result in a low resolution boundary with much of the noise is removed. The filtered boundary is then applied to Cullen et al. method to determine the tip width. The results are shown in Figure 31 using the red colour. The tip width is extracted manually and results are shown using the blue colour. The mathematical differences between the results produced manually and using this automatic method are shown in Figure 32.

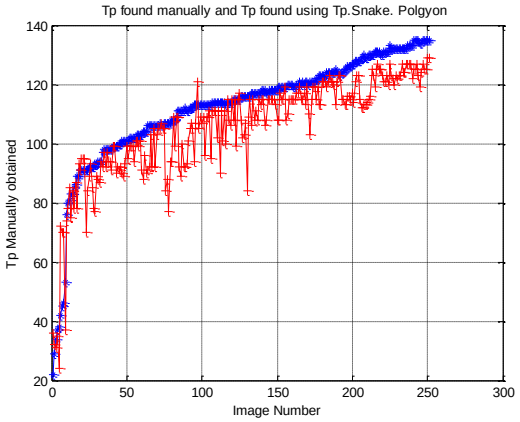

Fig. 31. Determining the tip width manually (shown in blue colour) and automatically using snake active contour, minimum perimeter polygon and Cullen et al. methods (shown in red).

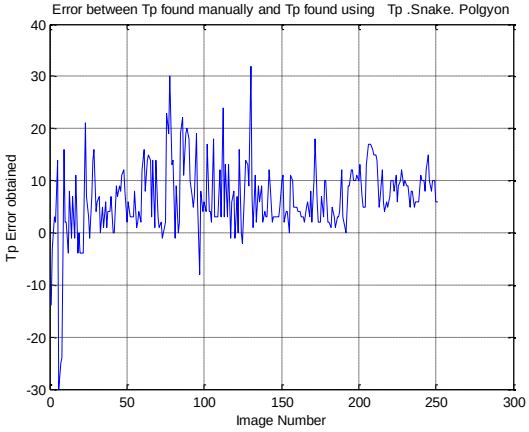

Fig.32. The error between estimating the tip width manually and automatically using snake active contours, minimum perimeter polygon and Cullen et al. methods.

We have calculated the standard deviation for errors shown in Figures 28, 30 & 32. The results are shown in the table below. The results in this table reveal that the snake algorithm, Fourier transform boundary descriptor and Cullen et al. methods gave the most accurate estimation for the tip width. On the other hand, the snake algorithm and Cullen et al. methods produces the worst estimation results for the tip width.

V. DISCUSSION OF THE RESULTS

In order to assess the performance of the nine techiniques that have been used to automatically determine the width of the spot welding electrode tip, the root mean square error has been calculated for the difference between the manually and automaticaly determined tip width sin pixels for the two hundred and fifty images in the image expermints. The results are shown in Table 4.1. The results that are presented in The results that are presented in this table reveal that the combination of the region growing technique, Minimum Perimeter Polygon approach and the Cullen et al's method is the most accurate method for determining the tip width for

250 experiments images the root meas square error is 7.5 % amongst the nine different combinations that have been discussed above. On the other hand, the GraphTheory algorithm, Fourier transforms and Cullen et al's method produces the high error of the nine combinations, because root mean square error is 43 % in this case for 250 experiments images.

Table 4.1 combination for Flat tip in RMSE

Combination	Cases	Root mean square error (RMSE) for 250 images	RMSE % for 250 images
1	Canny algorithm and Cullen et al method	87.7	35%
2	Canny Algorithm, Fourier Transform and Cullen et al method	92	36.8 %
3	Canny Algorithm , Minimum – Perimeter Polygon and Cullen et al method	107	42.8 %
4	Region grown Algorithm and Cullen et al method	45.7	18.2 %
5	Region grown Algorithm, Fourier Transform and Cullen et al method	65	26 %
6	Region grown Algorithm, Minimum – Perimeter Polygon and Cullen et al method	18.8	7.5 %
7	Graph Theory Algorithm and Cullen et al method	66.9	26.7 %
8	Graph Theory Algorithm, Fourier transform and Cullen et al method	107.9	43 %
9	Graph Theory Algorithm, Minimum – Perimeter Polygon and Cullen et al method	22.7	9%

For the three different algorithmic combinations that have been investigated in this section, the root mean square error was calculated for the respective errors in pixels between the automatic and manual tip width measurements (that were shown in figs 26 28 30). The results are shown in Table 4.2 the results in this table reveal that the combination of the Snake algorithm, Fourier transform boundary descriptor technique and Cullen et al.'s methods gave the most accurate automatic estimation for the size of the tip width. On the other hand, the combination of Snake algorithm, the combination of the Minimum Perimeter Polygon approach and Cullen et al.'s method produces the bad results for the automatic determination of the electrode tip width, although the overall variance between the three different combinations was relatively not small.

Table 4.2 Combination for Dome tip in RMSE

Combination	Cases	Root mean square error (RMSE) for 250 images	RMSE % for 250 images
1	Snake active contour and Cullen et al. methods.	9.5	3.6%
2	Snake active contour, Fourier transform boundary descriptor and Cullen et al. methods.	7.2	2.9%
3	Snake active contour and minimum perimeter polygons and Cullen et al.	59	23.6%

	methods.		

VI. C0NCLUSION

In this work, we have successfully designed an image processing algorithm to automatically determine the tip width for the anode. It is the anode quality that mainly determines the overall quality of the spot welding nugget [5]. In this paper, we proposed the use of a machine vision and image processing approach in order to determine the tip width automatically. The image processing process consists of three stages. The first stage is image segmentation for example using Canny algorithm, region growing, and Graph Theory approaches. The second stage involves boundary filtering, for example, the Fourier transform, or Minimum-Perimeter Polygon techniques. The last stage is that of boundary processing using the Cullen et al's method to automatically measure the tip width. These three stages produce nine different potential combinations of algorithms that may be used to automatically measure the tip width. This paper has shown that it is possible to perform the analysis of the spot welding electrode tip automatically. This information can be used to determine when to redress the electrode tip. This method of performing the tip width analysis has been carried out on a tapered tip. We have identified a combination of candidate image processing algorithms that works well with the set of two hundred and fifty images that we have in the image experiments. Initially many different image processing algorithms were investigated, and the candidate algorithms that are described here in detail are the best of those that were investigated, the others being discarded at an early stage. The best combination from amongst these candidates was then determined experimentally. This method is the region growing algorithm, with the Minimum–Perimeter Polygon approach and the Cullen et al's method. This method has the lowest root mean square error 7.5 % amongst all of the nine combinations that were investigated.

This paper has revealed that the Snake active contours method with Hybrid Level set model, combined with the Fourier transform boundary descriptor approach and Cullen et al method gives the best results for automatically estimating the electrode tip widths for dome –shaped spot welding electrodes. This method has the lowest root mean square error 2.9% amongst all of the three different algorithmic combinations that were investigated. The Snake active contours method with Hybrid Level set model gave best result

References

1 [1] X. Sun, ''Effect of projection height on projection collapse and nugget formation-finite element study'' *Welding Journal* , September 2001,pp.211-s-216-s

[2] H.D. Orts ''The Effects of Tic composite coating in Resistance Spot welding Galvanized Steel'' *Master Thesis*, Ohio state University, 1967.

[3] C. SM Nealon,L.S.H.lake ''Resistance spot welding tip lives for zincalume coated qualities, BHP steel research and technology centre'' *research report no 950*,January 1987.

[4] R.W. Jud ''Joining Galvanised and galvanneal steels'' *SAE Technical paper series*, No 840285, 1984.

[5] A. Morita, S. Inour, and A. Takezoe A ''Spot weldability of zinc vapour deposited steel sheets'' *Journal of metal finishing society*, Japan. Vol.39, No. 5, pp.270-275.

[6] L.M. Friedman, R.B. McCauley ''Influence of Metallurgical Characteristics on Resistance welding of Galvanized steel'' *welding Journal, supplement* ,Oct.1969, pp.454-462s.

[7] T. Saito.'' Resistance weldability of coated sheet for automotive application'' *Journal welding international* 1992, vol.6 No.9, pp695-699

[8] A. Mason, J.D.Cullen, A.I.AI-Shmma, W.Lucas''Real time image processing of electrode profile in resistance spot welding''. *Journal of Physics*: Conference Series, ISSN: 1742-6588, Vol. 15, pp.336-3441, 2005.

[9] A.Shi and J.Malik ''Normalized cuts and image segmentation '*' IEEE Transactions on pattern* analysis and machine intelligence, vol.22, No.8 August 2000

[10] R.C. Gonzalez, R.E.Woods, and S.L.Eddins'' Digital Image Processing using MATLAB'' *ISBN* 0-13-008519-7.2004

[12] D.Cullen, N. Athi, A.M. Al-Jader, A. Shaw. A and A. Al-Shamma'a '' Energy Reduction For The Spot Welding Process In The Automotive Industry '' Sensors And Their Applications XIV Conference (SENSORS07), Liverpool, UK, 11–13 September 2007, *Journal of Physics*: Conference Series, ISSN: 1742-6588, Vol. 76, IOP Publishing, Article No. 012022, 2007

[13] R Adams , L Bischof , "Seeded Region Growing''. *IEEE Transactions on Pattern Analysis and Machine Intelligence*, Vol. 16. IEEE Computer Society, Los Alamitos California, pp. 641–647, (1994)

[14] BS EN 25821:1992, ''Resistance spot welding electrode caps'', *British Standards Institute*

[15] BS 1140:1993: ''Specification for Resistance spot welding of uncoated and coated low carbon steel'', *British Standards Institute*

[16] RWMA Handbook, Fourth Edition, 1989

[17] J.D.Cullen, N.Athi, M.AL-Jader, P.Johnson, A.I.AL-Shamma,a, A.Shaw, A.M.A.EL-Rasheed, ''Multisensor fusion for on line monitoring of the quality of spot welding in automotive industry'' *Journal paper* ,Measurement, Vol 41, Issue 4, pp.412-423, 2008. ISSN: 0263-2241.

[18] S Szénási "Distributed Region Growing Algorithm for Medical Image Segmentation", *International Journal of Circuits, Systems and Signal Processing*, 2014, Vol. 8, No. 1, pp.173-181, ISSN 1998-4464

[19] "Z. Kerekes, Z. Toth, S. Szenasi, Z. Vamossy, Sz. Sergyan, ''Colon Cancer Diagnosis on Digital Tissue Images'' *Proceedings of IEEE 9th International Conference on Computational* Cybernetics. Tihany, 2013, pp. 159-163."

[20] S Szénási., "Distributed Implementations of Cell Nuclei Detection Algorithm", Recent Advances in Image, Audio and Signal Processing, *WSEAS* Press, Budapest, 2013, pp. 105-109.

[21] M. Kass, A. Witkin, and D. Terzopoulos, " Snakes: Active contour models," *Int. J. Comput. Vis.*, vol. 1, pp.321-331,1987

[22] D. Terzopoulos and K. Fleischer, "Deformable models," *Vis Comput*, vol. 4, pp. 306-331, 1988.

[23] T. McInerney and D. Terzopoulos, "A dynamic finite element surface mode for segmentation and tracking in multidimensional medical images with application to cardiac 4D image analysis," *Comput. Med. Imag. Graph*, vol. 19, pp. 69-83, 1995

[24] F. Leymarie and M. D. Levine, "Tracking deformable objects in the plane using an active contour model," IEEE Trans. Pattern Anal. *Machine Intell.*, vol. 15, pp. 617-634, 1993.

[25] R. Durikovic, K. Kaneda, and H. Yamashita, "Dynamic contour: A texture approach and contour operations, "*Vis. Comput*., vol. 11, pp.277-289,1995

[26] D. Terzopoulos and R. Szeliski, "Tracking with Kalman snakes," in *Active Vision*, A. Blake and A. Yuille, Eds. Cambridge, MA: MIT press, 1992, pp. 3-20

[27] V. Caselles, F. Catte, T. Coll, and F. Dibos, " A geometric model for active contours," *Numer. Math*., vol. 66, pp. 1-31, 1993